Numerical studies of slow rhythms emergence in neural microcircuits: Bifurcations and stability

Cite as: Chaos **19**, 015107 (2009); https://doi.org/10.1063/1.3096412
Submitted: 02 December 2008 . Accepted: 09 February 2009 . Published Online: 31 March 2009

M. A. Komarov, G. V. Osipov, J. A. K. Suykens, and M. I. Rabinovich

Numerical studies of slow rhythms emergence in neural microcircuits: Bifurcations and stability

M. A. Komarov,[1,2] G. V. Osipov,[1,2] J. A. K. Suykens,[2] and M. I. Rabinovich[3]
[1]*Department of Control Theory, Nizhny Novgorod University, 23 Gagarin Avenue, 603950 Nizhny Novgorod, Russia*
[2]*ESAT-SCD/SISTA, K.U. Leuven, Kasteelpark Arenberg 10, B-3001 Leuven (Heverlee), Belgium*
[3]*Institute for Nonlinear Science, University of California, San Diego, 9500 Gilman Drive 0402, La Jolla, California 92093-0402, USA*

(Received 2 December 2008; accepted 9 February 2009; published online 31 March 2009)

There is a growing body of evidence that slow brain rhythms are generated by simple inhibitory neural networks. Sequential switching of tonic spiking activity is a widespread phenomenon underlying such rhythms. A realistic generative model explaining such reproducible switching is a dynamical system that employs a closed stable heteroclinic channel (SHC) in its phase space. Despite strong evidence on the existence of SHC, the conditions on its emergence in a spiking network are unclear. In this paper, we analyze a minimal, reciprocally connected circuit of three spiking units and explore all possible dynamical regimes and transitions between them. We show that the SHC arises due to a Neimark–Sacker bifurcation of an unstable cycle. © *2009 American Institute of Physics*. [DOI: 10.1063/1.3096412]

The validity of dynamical models can be confirmed only when their solutions explaining the investigated phenomenon are structurally stable. An exhaustive sweep over the control parameters enlightens both regions of such solutions in the parameter space and, more interestingly, the evolution of the behavioral qualities along a particular change in parameters. Motivated by recent experimental observations that brain rhythms are products of local inhibitory networks, we have analyzed the dynamics of a minimal inhibitory circuit of three neurons. The considered microcircuit is capable of generating a global rhythm that does not depend on the details of the spiking activity in individual units. We have shown that the mathematical image of this behavior is a closed heteroclinic channel enclosing contour of saddle limit cycles and the heteroclinic orbits connecting them. Our bifurcation analysis yields the conditions on the emergence and the structural stability of this regime.

I. INTRODUCTION

The appearance and timing relationship of oscillatory activities with strongly different frequencies in complex neural systems and in the brain is one of the key problems of neuroscience. Many experiments indicate that spiking and bursting dynamics are involved in different ways in neuronal microcircuit functions and in brain rhythm generation.[1–4] In particular, spiking (temporal) and bursting (rate) activity can be independent and code for different entities or sensory variables.[5] What is the dynamical origin of the slow rhythm generation? We analyzed the minimal inhibitory neural circuit of spiking neurons that is modeled by Bonhoeffer–Van der Pol equations. We showed here that subcritical Neimark–Sacker bifurcation leads to the appearance of structurally stable heteroclinic channel (SHC). The skeleton of this channel is a heteroclinic contour that consists of saddle limit cycles and the heteroclinic orbits connecting them. It happens when the degree of the nonsymmetry of the network connectivity exceeds a critical level.

Similar problems have been investigated in Ref. 6. The authors of that work compared the bifurcation sequence from tonic spiking activity to burst generation in an inhibitory network of Hodgkin–Huxley neurons with the sequence of qualitative transformations of the phase portrait that leads to the appearance of a heteroclinic cycle in the framework of a time-averaged (rate) model of the same network and found that these sequences are the same. In this paper we directly calculate the Floquet multipliers of limit cycles and determine the critical parameter values when two complex conjugate multipliers reach unit modulus. The observed bifurcation leads to the appearance of a structurally stable regime of the sequential switching of the activity of spiking neurons. Due to structural stability, slow rhythm generation practically does not depend on the neural model. It only depends on the connectivity parameters. However, to investigate the bifurcations in detail, we need to use a rather representative model on the one hand, but also rather convenient for analysis on the other hand.

II. NETWORK MODEL

We consider the network of three spiking neurons (shown in Fig. 1), modeled by the Bonhoeffer–Van der Pol equations,

$$\tau_1 \frac{dx_i(t)}{dt} = x_i - \frac{1}{3}x_i^3(t) - y_i(y) - z_i(t)(x_i(t) - v) + S_i,$$
$$\frac{dy_i(t)}{dt} = x_i(t) - by_i(t) + a, \quad i = 1, \ldots, 3, \tag{1}$$

synaptically inhibitory connected through the coupling $z_i(t)$, which is defined by

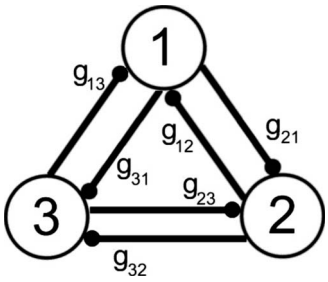

FIG. 1. Neuronal network: motif of three reciprocally inhibitory coupled neurons.

$$\tau_2 \frac{dz_i(t)}{dt} = \sum_j g_{ij} F(x_j) - z_i(t). \tag{2}$$

Here $x_i(t)$ denotes the membrane potential of the ith neuron, $y_i(t)$ the variable corresponding to the action of all ionic currents, S_i the external stimuli to each neuron, v the reversal potential, g_{ij} the coupling coefficients between the ith and jth neuron and $F(x_j)=1/(1+\exp((0.5-x_j)/20))$. The values of the parameters are fixed in all simulations to $a=0.7$, $b=0.8$, $\tau_1=0.08$, $\tau_2=3.1$, and $v=-1.5$, and we chose the parameter $S_i>0.35$ that corresponds to tonic spiking regime of individual uncoupled neurons. Depending on the level of nonsymmetry of inhibitory coupling, this simple network demonstrates the variety of dynamical regimes.

- One neuron is active (spiking oscillations) and two other neurons are suppressed (subthreshold oscillations). Time series is shown in Fig. 2(a).
- Two neurons are active (spiking oscillations) and one neuron is suppressed (subthreshold oscillations). Time series is shown in Fig. 2(b).
- The regime of synchronous in-phase spiking oscillations of all three neurons ($x_1=x_2=x_3$). Time series is shown in Fig. 2(c).
- Various regimes of sequential activation of the neurons. Time series are shown in Figs. 2(d)–2(f).

III. DISTRIBUTION OF THE CONTROL PARAMETERS SPACE

Figures 3(a) and 3(b) present the bifurcation diagram in the plane (g_1, g_2) of the regimes in systems (1) and (2). For better representation of the main results we assume $g_1=g_{12}=g_{23}=g_{31}$ for a clockwise coupling, and $g_2=g_{13}=g_{32}=g_{21}$ for a counterclockwise coupling. Because of identical neurons in the ensemble, the diagram is symmetric with respect to the diagonal line, which is characterized by $g_1=g_2$. Figure 3(b) is the detailed area in Fig. 3(a). At sufficiently large and symmetric ($g_1 \approx g_2$) couplings (region A), six limit cycles can be observed. First, three limit cycles (we denote them $L^1_{1,2,3}$) correspond to the dynamics when one of the three neurons produces periodic spikes and suppresses the spiking activity of the two other neurons [Fig. 2(a)].

Second, three limit cycles (we denote them $L^2_{1,2,3}$) correspond to the dynamics when one of the three neurons is suppressed (subthreshold oscillations) by the other two active (in-phase spiking oscillations) neurons [Fig. 2(b)]. At transition from region A to region B, the limit cycles $L^2_{1,2,3}$ on the curve h_2 disappear through the saddle-node limit cycle bifurcation (one of real multipliers reaches a value of +1). In region B, systems (1) and (2) have only three limit cycles $L^1_{1,2,3}$. In region C, in systems (1) and (2) there exists only one regime: periodical sequential activation of all neurons [Fig. 2(d)]. The transition from region B to region C (boundary line h_1) is very important because it corresponds to the most realistic values of the parameters: one coupling is sufficiently strong (strong inhibition) and the other coupling is rather small or absent. For this reason a detailed description of the bifurcation on line h_1 will be given now.

Region D is the region of coexistence of seven limit cycles: three limit cycles $L^1_{1,2,3}$, three limit cycles $L^2_{1,2,3}$, and one limit cycle corresponding to synchronous in-phase spiking oscillations of all three neurons [we denote it by L^3; the time series are shown in Fig. 2(c). In region E, four stable limit cycles can be observed: the three cycles $L^2_{1,2,3}$ and limit cycle L^3. The transition from D to E is accompanied by a subcritical Neimark–Sacker bifurcation of the limit cycles $L^1_{1,2,3}$. Region F has a complex structure. There are areas there that the three limit cycles $L^2_{1,2,3}$ coexist with the limit cycle L^3. In the rest there is the coexistence of the sequential dynamics and the stable limit cycle L^3. The transition from region E to region F leads to the disappearance of the three limit cycles $L^2_{1,2,3}$ through the saddle-node limit cycle bifurcation and the appearance of sequential dynamics. A more detailed description of such a transition will be given below. In region G, only the limit cycle L^3 corresponding to identical behavior ($x_1=x_2=x_3$) is stable.

On the boundary of curve h_3 (transition from F to G), the limit cycle corresponding to the sequential dynamics disappears. One of the multipliers of this cycle reaches the value of -1, i.e., the stable limit cycle merges with the saddle limit cycle of doubled period. However, on the top boundary of region F (curve h_4), limit cycle L^3 loses stability via a subcritical Neimark–Sacker bifurcation. Finally on the curve h_2, between regions E and G, three limit cycles $L^2_{1,2,3}$ disappear through the saddle-node bifurcation. Hence, region G is the region where only one limit cycle L^3 exists. Systems (1) and (2) also have areas in the diagram (Fig. 3) where there exist three limit cycles which correspond to the antiphase synchronous spiking activity of two neurons and the subthreshold oscillation of one neuron.

IV. NEIMARK–SACKER BIFURCATION: EMERGENCE OF HETEROCLINIC SEQUENCE

In order to study the bifurcation leading to the appearance of the regime of sequential switching on line h_1 [Fig. 3(a)], we calculated the dependencies of the multipliers of the limit cycles on the relation of coupling coefficients $\alpha_i=g_{ij}/g_{ji}$, where g_{ij} are the coefficients of the clockwise coupling and g_{ji} are the coefficients of the counterclockwise coupling (in experiments the coefficients of the counterclockwise coupling remain constant and are equal to 0.5). It was found that the pair of complex multipliers $\mu_{1,2}$ of the limit cycle L^1_1 (further denoted by L_1) reaches the unit modulus with a decrease in the relation of synaptic couplings $\alpha_1=g_{12}/g_{21}$ (Fig. 4).

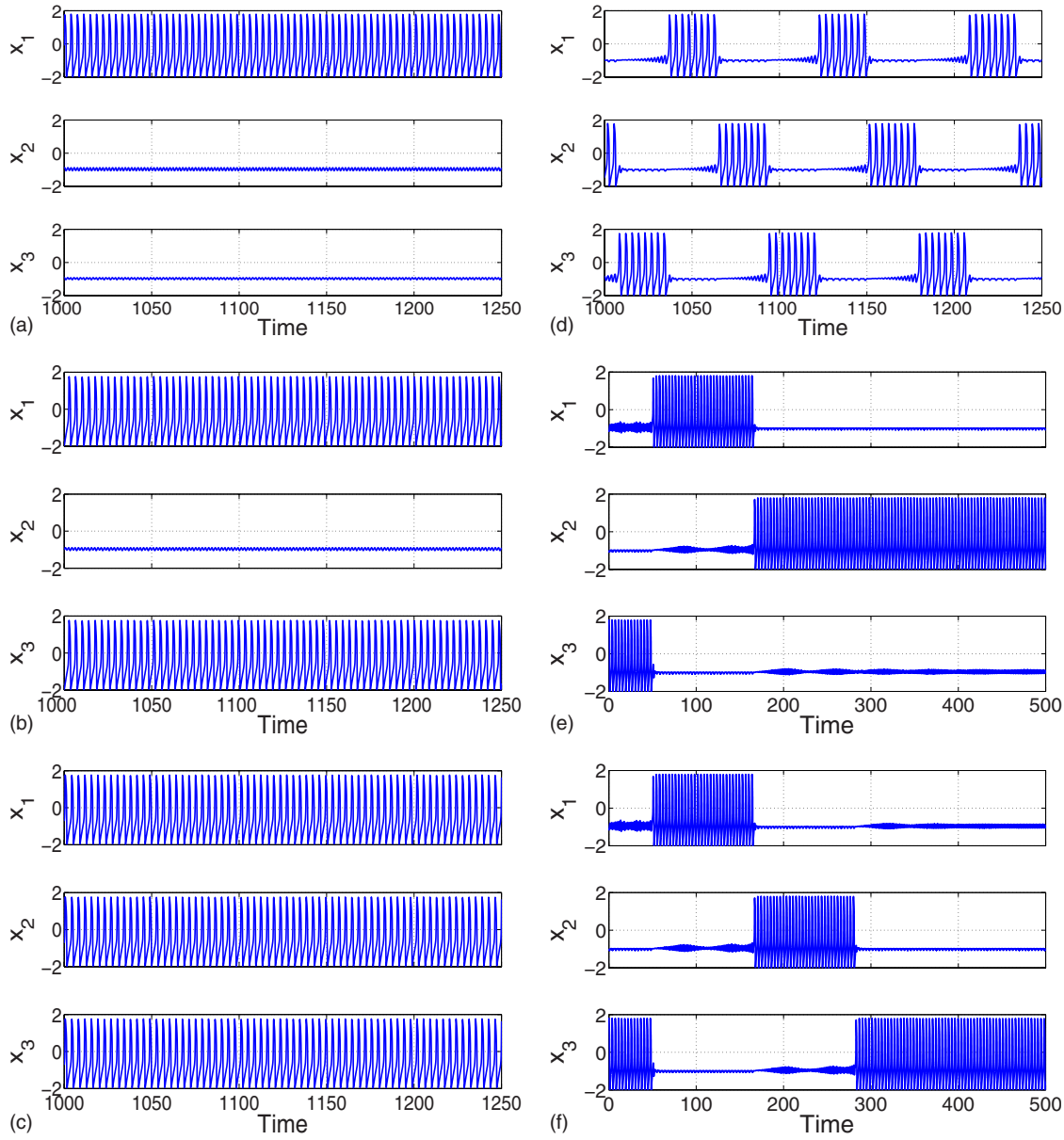

FIG. 2. (Color online) (a) One neuron is active and suppresses the activity of the two other neurons. Parameters: $g_{ij}=g_{ji}=0.5$ and $i,j=1,\ldots,3$. (b) Two neurons are active and suppress the activity of the other neuron Parameters: $g_{ij}=g_{ji}=0.3$ and $i,j=1,\ldots,3$. (c) Synchronous in-phase ($x_1=x_2=x_3$) spiking mode. Parameters:$g_{ij}=g_{ji}=0.03$ and $i,j=1,\ldots,3$.; (d) Periodical sequential activation of the neurons. Parameters: $g_{12}=g_{23}=g_{31}=0.5$, $g_{21}=g_{13}=g_{32}=0.05$, and ($\alpha_1=\alpha_2=\alpha_3=0.1$). [(e) and (f)] Transient sequential activation of the neurons. Parameters: (e) $g_{12}=0.06$, $g_{23}=0.07$, $g_{31}=0.0732$, $g_{21}=g_{32}=g_{13}=0.5(\alpha_1=0.12$, $\alpha_2=0.1404$, $\alpha_3=0.1464)$. (f) $g_{12}=g_{23}=0.06$, $g_{31}=0.0732$, $g_{21}=g_{32}=g_{13}=0.5(\alpha_1=\alpha_2=0.12$, $\alpha_3=0.1464)$.

The eigenvectors of the monodromy matrix corresponding to the multipliers $\mu_{1,2}$ depend only on x_2 and y_2. Therefore we are able to introduce Poincaré section which allows us to study the possible bifurcation in systems (1) and (2) in detail. Mapping of the plane $\Pi_1=\{x_1=0,\ y_1=-0.18,\ z_1=0,\ z_2=0.01,\ x_3=-0.9,\ y_3=-0.32,\ z_3=0.018\}$ to itself (all values of the variables were chosen on the limit cycle L_1 except the variables x_2,y_2) allows us to detect the existence of the saddle torus T_1. Figure 5 shows the sections of the saddle torus T_1 with the plane Π_1.

From region A [Fig. 5(a)], all trajectories go to the stable limit cycle L_1 (infinite spiking oscillation of the first element, i.e., fixed point in mapping of plan Π_1 to itself). From region B, all trajectories go to the stable limit cycle L_2 (infinite spiking oscillations of the second element). When decreasing α_1, the saddle torus T_1 goes to the stable limit cycle L_1, and at the bifurcation value of α_1, it merges with the limit cycle and passes its instability [Fig. 5(b)]. Thus, a subcritical Neimark–Sacker bifurcation takes place.[7] The numerical investigation of different initial conditions shows that before the bifurcation all trajectories from the vicinity of the unstable saddle torus go to the stable limit cycle L_1 or to the stable limit cycle L_2 [Figs. 5(a), 5(F), 5(i), 5(g), and 7]. Figure 6 shows the unstable torus T_1 and the stable limit cycle L_1 in the subspace of the transformed coordinates $\xi_1=x_1+x_2\cos(\theta)$,
$\xi 2=\mathrm{y1}+\mathrm{x2}\sin(\theta)$, $\xi 3=\mathrm{y2}+10\mathrm{z1}$, $\theta=\mathrm{arctg}(\mathrm{y}'1/\mathrm{x}'1)$.

Figure 7 shows a few trajectories that go from the vicinity of the unstable torus T_1 to the stable limit cycle L_2. For a better representation, the trajectories were plotted in two sub-

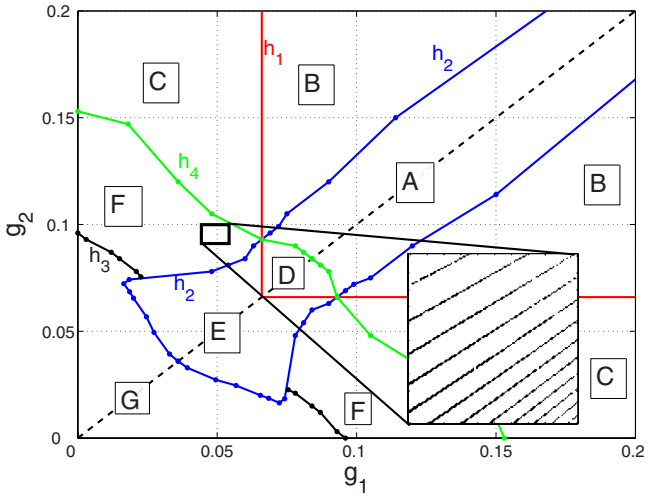

FIG. 3. (Color online) Bifurcation diagram of regimes in an ensemble of three inhibitory coupled neurons. Region A: coexistence of three limit cycles $L^1_{1,2,3}$ [Fig. 2(a)] and three limit cycles $L^2_{1,2,3}$ [Fig. 2(b)]. Region B: coexistence of three limit cycles $L^1_{1,2,3}$. Region C: periodic sequential switching of activity between all neurons [Fig. 2(c)]. Region D: coexistence of three limit cycles $L^1_{1,2,3}$, three limit cycles $L^2_{1,2,3}$, and limit cycle L^3 [Fig. 2(d)]. Region E: coexistence of three limit cycles $L^1_{1,2,3}$ and limit cycle L^3. Region F: region with complex structure. The black areas in the inserted figure correspond to the coexistence of the three limit cycles $L^2_{1,2,3}$ with the limit cycle L^3. The white regions are the areas of the coexistence of the sequential dynamics and the stable limit cycle L^3. Region G: the existence of limit cycle L^3.

spaces: the trajectories situated near T_1 [subspace (ξ_1,ξ_2,ξ_3)] and phase points going to the stable limit cycle L_2 [subspace $(x_2+x_1,y_2,10z_1)$].

It is necessary to notice that such bifurcation is typical for the other limit cycles L_2 and L_3. With decreasing g_{23} and g_{31}, the subcritical Neimark–Sacker bifurcation takes place for L_2 and L_3 correspondingly. The behavior of the trajectories at $\alpha_1=0.1384$, $\alpha_2=0.1404$, and $\alpha_3=0.1464$ (before bifurcations of each limit cycle $L_{1,2,3}$) is illustrated in Fig. 8. The red curves t_2 and t_3 are the intersections of the saddle tori T_2 and T_3 with planes Π_2 and Π_3 correspondingly (planes Π_2 and Π_3 were chosen in analogous way as Π_1). The black line with the arrow, which goes from T_1 to L_2, represents the set of trajectories that go from the vicinity of saddle torus T_1 to the stable limit cycle L_2 (Fig. 7).

In Refs. 8 and 9 it was shown that heteroclinic orbits and sequences of heteroclinic orbits between saddle points in the phase space of dynamical system are the mathematical image

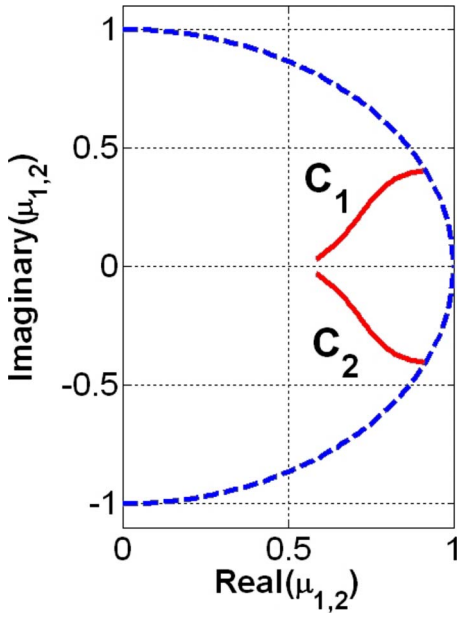

FIG. 4. (Color online) Real and imaginary parts of multipliers $\mu_{1,2}$ of the limit cycle L_1. At $\alpha_1\approx0.1362$, the absolute values of the multipliers are equal to 1.

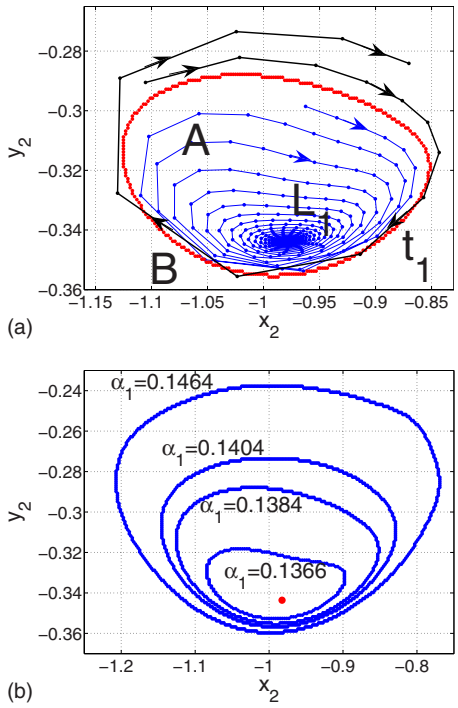

FIG. 5. (Color online) (a) Mapping of the plane Π_1 to itself. Red line t_1: intersection of the saddle torus T_1 with plane Π_1. From region A, all trajectories go to the stable limit cycle L_1 (infinite spiking oscillation of the first element, i.e., fixed point in mapping of the plane Π_1 to itself). From region B, all trajectories go the stable limit cycle L_2 (infinite spiking oscillations of the second element). $\alpha_1=\alpha_2=\alpha_3=0.1384$. (b) Intersections of the torus T_1 with plane Π_1 at different values of the coupling strength $\alpha_1=0.1464$, 0.1404, 0.1384, and 0.1366. When decreasing α_1, the saddle torus T_1 becomes closer to the stable limit cycle L_1, and at a bifurcation value of α_1, it merges with the limit cycle and passes it its instability.

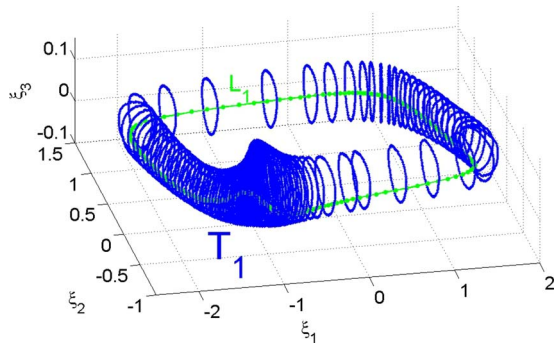

FIG. 6. (Color online) Illustration of the saddle torus T_1 and the stable limit cycle L_1 (green curve) in the subspace (ξ_1,ξ_2,ξ_3). The intersections (closed blue curves) of torus T_1 with different planes are shown.

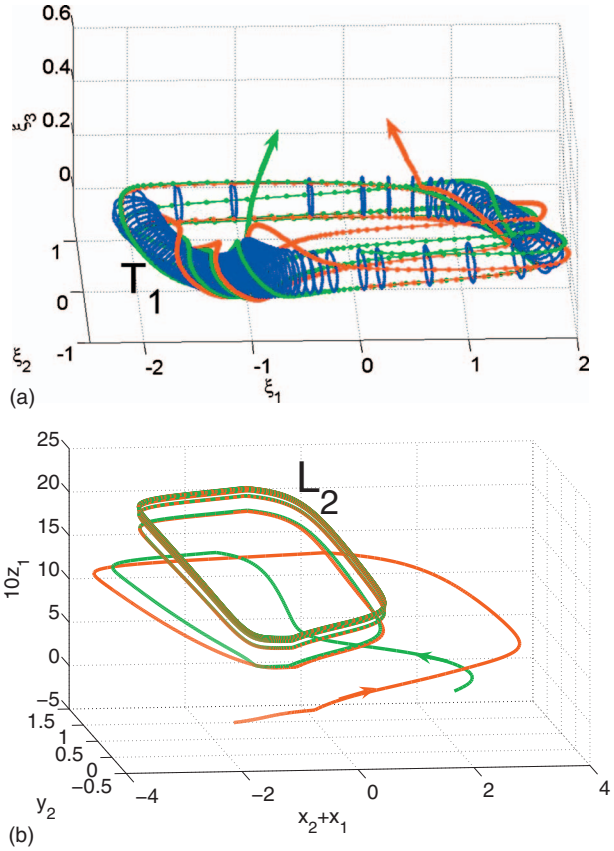

FIG. 7. (Color) (a) Saddle torus T_1 and a few trajectories going from the vicinity of T_1 to the stable limit cycle L_2. (b) Continuing of the trajectories plotted in (a): the trajectories go to the stable limit cycle L_2. Here $\alpha_1=\alpha_2=\alpha_3=0.1464$.

of sequential activity in the networks modeled by a modified Lotka–Volterra model (rate model). In our case the arising of stable heteroclinic orbits is also at the origin of the sequential firing. Let us consider the case when $\alpha_1 \approx 0.1362$ is approximately equal to the critical value when the subcritical Neimark–Sacker bifurcation takes place and the saddle torus T_1 merges with the stable limit cycle L_1. Before bifurcation, the set of trajectories goes from the vicinity of T_3 to L_1. Hence, at the moment of the bifurcation between the saddle torus T_3 and the unstable limit cycle L_1, the set of heteroclinic orbits appears. Such a set of heteroclinic orbits between saddle modes is the mathematical image in the phase space of the sequential switching of activity. The schematic illustrations of the trajectories and time series are shown in Figs. 9 and 2(e) correspondingly. The initial conditions in the vicinity of saddle torus T_3 [in region B in Fig. 5(a)] provide finite oscillations of the third element [Figs. 9 and 2(e)]. Next, due to the instability of the torus T_3, the phase point leaves the vicinity of T_3 near the heteroclinic orbit and goes to the unstable L_1 (black line with arrow in Fig. 9). Then, due to the instability of L_1, the phase point remains located at the vicinity of L_1 for a certain time. This fact provides finite oscillations of the first element and suppression of spiking oscillations in the other elements. Finally, the phase point leaves the vicinity of L_1 and goes to the stable limit cycle L_2 (infinite oscillations of the second element and suppression of the other elements). When further decreasing α_1, a heteroclinic orbit between T_3 and L_1 disappears but the switching behavior remains.[8,9] So we can claim the existence of a *SHC*.[10]

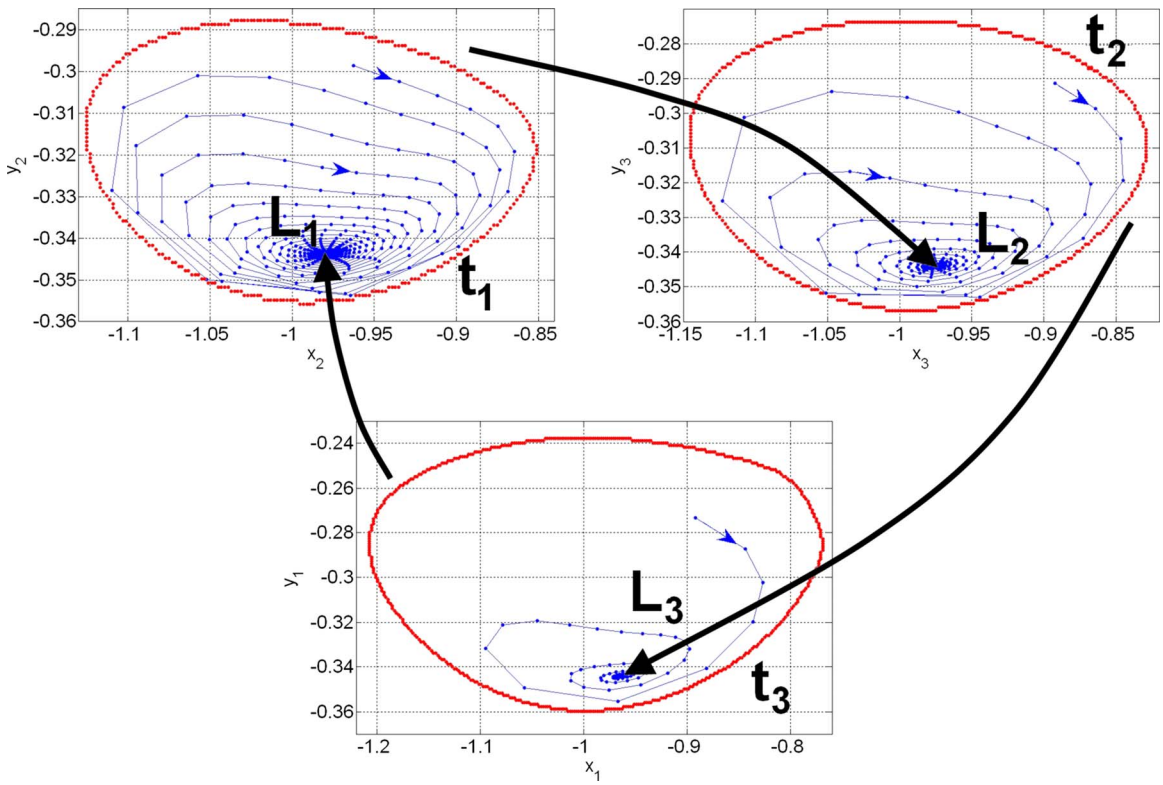

FIG. 8. (Color online) Schematic illustration of the trajectories at $\alpha_1=0.1384$, $\alpha_2=0.1404$, and $\alpha_3=0.1464$. The black lines with the arrows illustrate the set of trajectories going from the vicinity of the saddle tori to the stable limit cycles (Fig. 7).

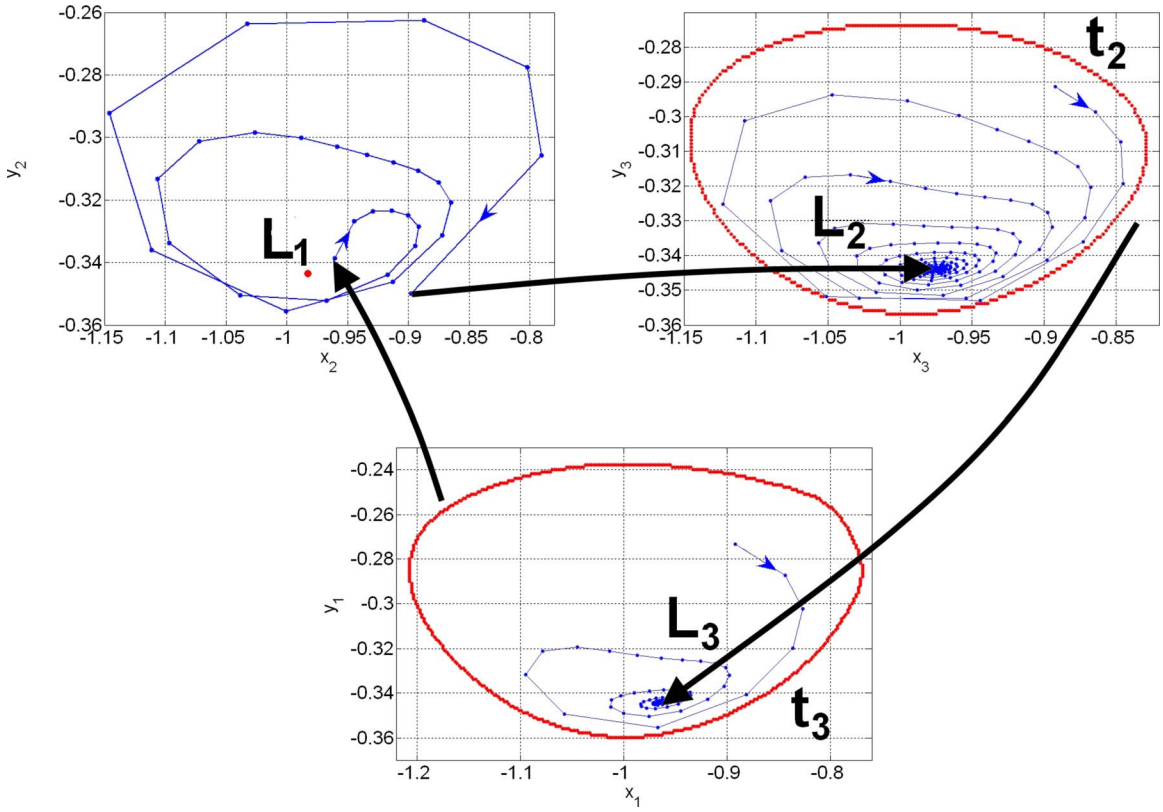

FIG. 9. (Color online) Illustration of the trajectories for $\alpha_1=0.1344$, $\alpha_2=0.1404$, and $\alpha_3=0.1464$. Sequential switching of the activity arising from a heteroclinic orbit formation [time series presented in Fig. 2(e)].

When simultaneously decreasing α_1 and α_2 to the bifurcation value, a sequence of heteroclinic orbits between saddle modes arises: (i) the heteroclinic orbit between saddle torus T_3 and the saddle limit cycle L_1 and (ii) the heteroclinic orbit between the saddle limit cycle L_1 and the saddle limit cycle L_2. Such a sequence also collapses when further decreasing α_1 and α_2, but the heteroclinic channel remains stable up to zero values of the coupling strength. Schematic presentations of the trajectories and the time series are shown in Figs. 10 and 2(f), respectively.

The generation of sequential activity is also finite in time, but now it covers all neurons. Let us notice that heteroclinic channels are constructions in the phase space capable at describing transient generation of bursting waves in neuronal ensembles, unlike stable limit cycles, which are images of periodic activity. Finally, simultaneous decrease in all three coupling coefficients g_{12}, g_{23}, and g_{31} leads to the formation of heteroclinic orbits between the saddle limit cycles L_1, L_2, and L_3. When further decreasing the conductances, the heteroclinic contour collapses and in its vicinity stable limit cycle appears. It is the image of a periodical sequential activity occurring in the ensemble [Figs. 11 and 2(d)].

Note that a similar bifurcation of the formation of a stable limit cycle, appearing as a destruction of the heteroclinical contour, is analytically studied in Refs. 6 and 8. On the boundary h_2 between regions E and F, a transition from the periodic dynamics to sequential switching activity was also observed. Remember that in region E three stable limit cycles $L^2_{1,2,3}$ coexist. Each limit cycle corresponds to the periodic spiking activity of two neurons and a subthreshold oscillation of the third neuron [the time series are shown in Fig. 2(b)]. It was found that in the phase space other three limit cycles exist. However they are saddle cycles. The stable manifolds of these cycles separate the basins of attractions of stable cycles $L^2_{1,2,3}$. When a decrease in the ratio g_1/g_2 on the boundary h_2, one of the multipliers of stable limit cycles reaches the value of +1. It means that each stable limit cycle merges with the saddle cycle. At this moment the heteroclinic contour arises.[6] When further decreasing g_1/g_2, this contour collapses and irregular behavior corresponding to sequential bursting activity is set, as shown in Fig. 12.

V. CONCLUSION

The modulation instability that is related to subcritical Neimark–Sacker bifurcation is a general mechanism of slow oscillation generation. In an inhibitory network with nonsymmetrical connections, the period of such slow oscillations is determined by cycling inhibition and does not depend on the details of the neuronal spiking activity. No one neuron can be pointed as the leader of the rhythm. This is a winnerless competition principle that has been suggested in Ref. 11. The results of this paper showed that the closed heteroclinic contour (mathematical image of sequential switching in the network of inhibitory coupled spiking neurons) is a structurally stable object.

The structural stability of the discussed slow oscillation is an important point for understanding the possible mechanisms of information processing in the brain. In particular, the interaction between spiking and bursting dynamics is de-

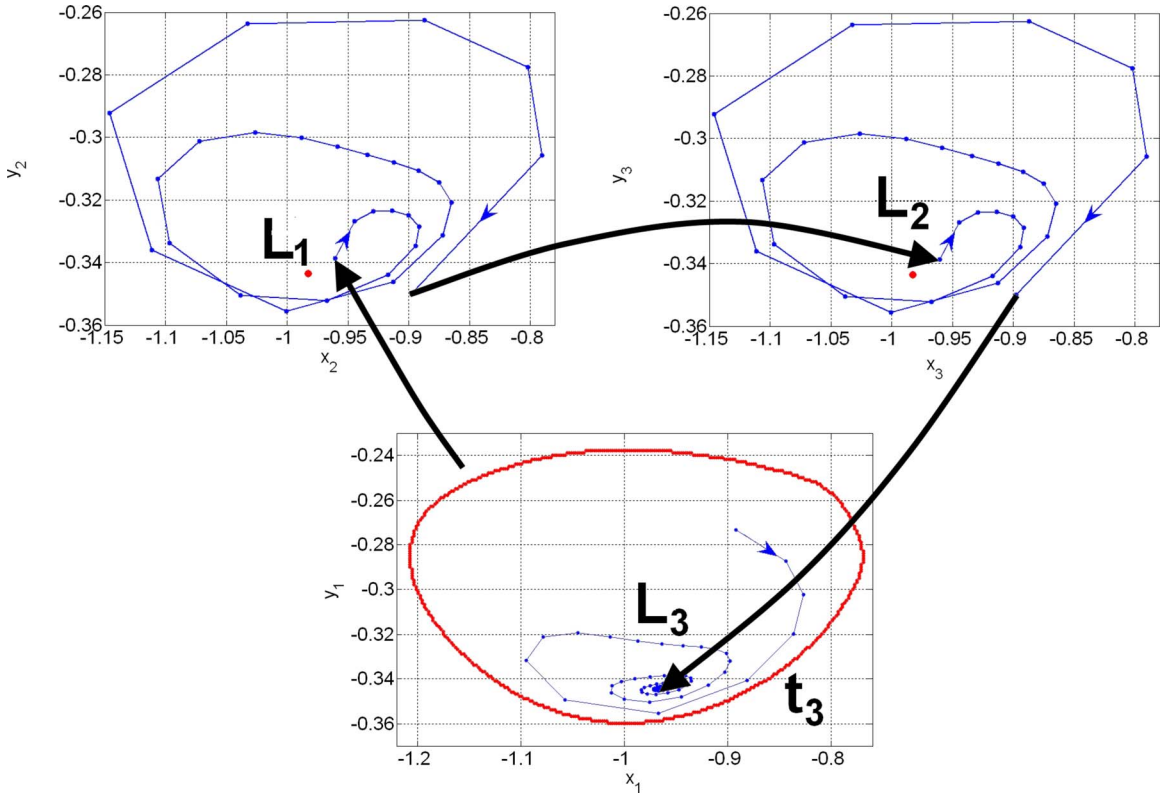

FIG. 10. (Color online) Trajectories corresponding to $\alpha_1=\alpha_2=0.1344$ and $\alpha_3=0.1464$. Sequential switching of the activity arising from a heteroclinic orbit formation [time series presented in Fig. 2(f)].

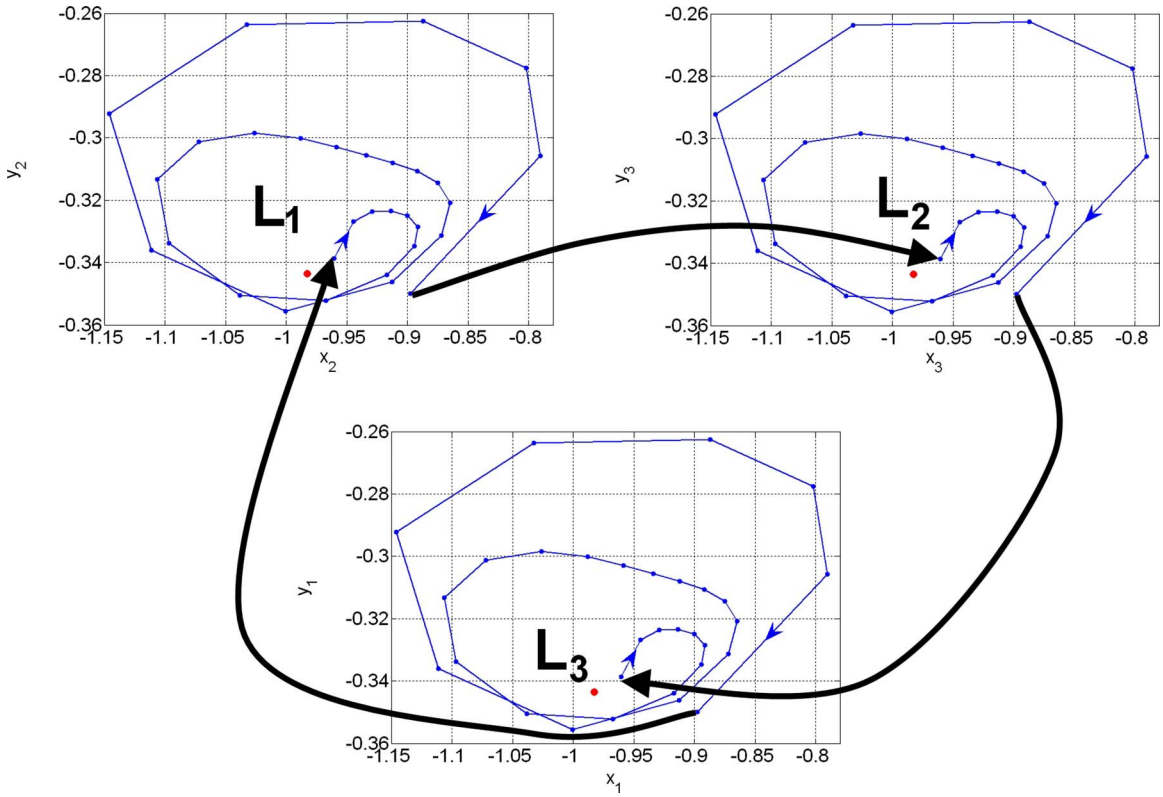

FIG. 11. (Color online) Trajectories corresponding to $\alpha_1=\alpha_2=\alpha_3=0.1344$. The periodic generation of sequential activity is shown [time series presented in Fig. 2(d)]. A limit cycle arises in the vicinity of the heteroclinic sequence between the saddle limit cycles.

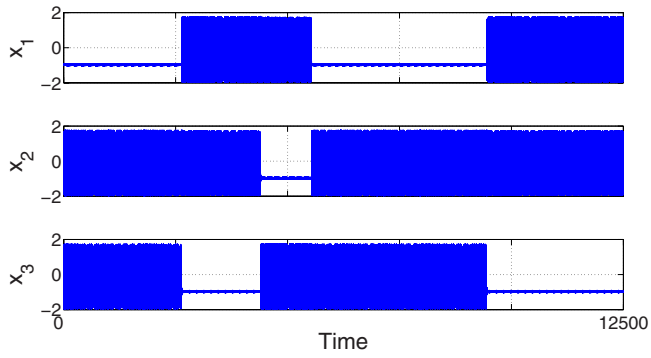

FIG. 12. (Color online) Irregular sequential activation of neurons in region F.

termined to be the mechanism of working memory, different coding strategies in the sensory systems, the mechanisms of motor command generation, and neural microcircuits coordination.[2] Synchronization of the ensemble of microcircuits, which generates the rhythm in different parts of the brain, can be the origin of different brain rhythms.[1]

While we have investigated a minimal inhibitory network in this paper, the phenomenon of sequential switching activity of spiking neurons between quasistationary states, which is typical for a heteroclinic contour, has been observed *in vivo* in the gustatory cortex[12] and other systems.[13]

ACKNOWLEDGMENTS

We thank V. Afraimovich and V. Belykh for fruitful discussions. This work is done with financial support from RFBR, under Project Nos. 06-02-16596, 08-02-97049, and 08-02-92004. J. A. K. Suykens acknowledges support from K. U. Leuven, the Flemish government, FWO, and the Belgian federal science policy office (FWO Contract No. G.0226.06, CoE Contract No. EF/05/006, GOA AMBioRICS, IUAP DYSCO, and BIL/05/43). M. I. Rabinovich acknowledges support from ONR under Grant No. N00014-07-1-0741.

[1] G. Buzsáki, *Rhythms of the Brain* (Oxford University Press, Oxford, 2006).
[2] M. I. Rabinovich, P. Varona, A. I. Selverston, and H. D. I. Abarbanel, Rev. Mod. Phys. **78**, 1213 (2006).
[3] R. H. R. Hahnloser, A. A. Kozhevnikov, and M. S. Fee, Nature (London) **419**, 65 (2002).
[4] O. Mazor and G. Laurent, Neuron **48**, 661 (2005).
[5] J. Huxter, N. Burgess, and J. O'Keefe, Nature (London) **425**, 828 (2003).
[6] T. Nowotny and M. I. Rabinovich, Phys. Rev. Lett. **98**, 128106 (2007).
[7] E. Ott, *Chaos in Dynamical Systems* (Cambridge University Press, Cambridge, 1993).
[8] V. S. Afraimovich, M. I. Rabinovich, and P. Varona, Int. J. Bifurcation Chaos Appl. Sci. Eng. **14**, 1195 (2004).
[9] V. S. Afraimovich, V. P. Zhigulin, and M. I. Rabinovich, Chaos **14**, 1123 (2004).
[10] M. I. Rabinovich, R. Huerta, P. Varona, and V. S. Afraimovich, PLOS Comput. Biol. **4**, e1000072 (2008).
[11] M. Rabinovich, A. Volkovskii, P. Lecandra, R. Huerta, H. D. I. Abarbanel, and G. Laurent, Phys. Rev. Lett. **87**, 068102 (2001).
[12] L. M. Jones, A. Fontanini, B. F. Sadacca, P. Miller, and D. B. Katz, Proc. Natl. Acad. Sci. U.S.A. **104**, 18772 (2007).
[13] M. Rabinovich, R. Huerta, and G. Laurent, Science **321**, 48 (2008).